Title

Temporal and spatial patterns of microbial community biomass and composition in the Southern California Current Ecosystem

Authors

Taylor, AG
Landry, MR
Selph, KE
et al.

Publication Date

2015-02-01

DOI

10.1016/j.dsr2.2014.02.006

Peer reviewed

Deep-Sea Research II 112 (2015) 117–128

Contents lists available at ScienceDirect

Deep-Sea Research II

journal homepage: www.elsevier.com/locate/dsr2

Temporal and spatial patterns of microbial community biomass and composition in the Southern California Current Ecosystem

Andrew G. Taylor [a,*], Michael R. Landry [a], Karen E. Selph [b], John J. Wokuluk [a]

[a] Scripps Institution of Oceanography, University of California at San Diego, La Jolla, CA 92093-0227, USA
[b] Department of Oceanography, University of Hawaii at Manoa, Honolulu, HI 96822, USA

ARTICLE INFO

Available online 18 February 2014

Keywords:
California Current Ecosystem
Microbial community
Plankton biomass
Epifluorescence microscopy
Flow cytometry
Carbon to chlorophyll ratio

ABSTRACT

As part of the California Current Ecosystem Long Term Ecological Research (CCE-LTER) Program, samples for epifluorescence microscopy and flow cytometry (FCM) were collected at ten 'cardinal' stations on the California Cooperative Oceanic Fisheries Investigations (CalCOFI) grid during 25 quarterly cruises from 2004 to 2010 to investigate the biomass, composition and size–structure of microbial communities within the southern CCE. Based on our results, we divided the region into offshore, and inshore northern and southern zones. Mixed-layer phytoplankton communities in the offshore had lower biomass (16 ± 2 μg C L^{-1}; all errors represent the 95% confidence interval), smaller size-class cells and biomass was more stable over seasonal cycles. Offshore phytoplankton biomass peaked during the winter months. Mixed-layer phytoplankton communities in the northern and southern inshore zones had higher biomass (78 ± 22 and 32 ± 9 μg C L^{-1}, respectively), larger size-class cells and stronger seasonal biomass patterns. Inshore communities were often dominated by micro-size (20–200 μm) diatoms; however, autotrophic dinoflagellates dominated during late 2005 to early 2006, corresponding to a year of delayed upwelling in the northern CCE. Biomass trends in mid and deep euphotic zone samples were similar to those seen in the mixed-layer, but with declining biomass with depth, especially for larger size classes in the inshore regions. Mixed-layer ratios of autotrophic carbon to chlorophyll *a* (AC:Chl *a*) had a mean value of 51.5 ± 5.3. Variability of nitracline depth, bin-averaged AC:Chl *a* in the mixed-layer ranged from 40 to 80 and from 22 to 35 for the deep euphotic zone, both with significant positive relationships to nitracline depth. Total living microbial carbon, including auto- and heterotrophs, consistently comprised about half of particulate organic carbon (POC).

1. Introduction

The California Current Ecosystem (CCE) is a productive eastern boundary current system where nutrient delivery by coastal upwelling, wind stress curl and mesoscale eddies support high plankton production and standing stocks (Huyer, 1983; Legaard and Thomas, 2006; Rykaczewski and Checkley, 2008; Mantyla et al., 2008; Thomas et al., 2009). The main core of the California Current flows equatorward along the west coast of North America, and is defined by cool, low salinity subarctic water (Hickey, 1979; Lynn and Simpson, 1987). In the southern portion of the CCE Point Conception marks a transition zone, as the primary orientation of the coast line abruptly shifts from north–south to east–west, becoming the northern portion of the Santa Barbara Basin (SBB). A poleward flowing California Undercurrent originates in the eastern tropical Pacific, bringing warm, saline water from offshore and the south and forming the Southern California eddy which is centered approximately near San Nicholas Island (Lynn and Simpson, 1987; Niiler et al., 1989; Bray et al., 1999). The interactions of these currents in the California Bight and offshore regions set up distinct floristic zones, defined by water masses and floral patterns, that can be used to split the region into northern and southern nearshore, and offshore regions (Hayward and Venrick, 1998; Venrick, 2002, 2009).

To better understand pelagic ecosystem dynamics of the southern CCE, extensive modeling and remote sensing studies have been conducted to determine processes controlling chlorophyll *a* concentrations, primary production, phytoplankton growth rates, biomass and carbon to chlorophyll *a* ratios (Eppley et al., 1985; Peláez and McGowan, 1986; Di Lorenzo et al., 2004; Gruber et al., 2006; Li et al., 2010; Kahru et al., 2012, 2015). However, the success of such studies depends highly on quality in situ measurements for parameterization, algorithm development and validation.

The California Cooperative Oceanic Fisheries Investigations (CalCOFI) has conducted routine assessments of ocean hydrography and biology on a spatially extensive sampling grid pattern in

* Corresponding author. Tel.: +1 858 534 6097; fax: +1 858 534 6500.
E-mail address: agtaylor@ucsd.edu (A.G. Taylor).

http://dx.doi.org/10.1016/j.dsr2.2014.02.006
0967-0645

the southern CCE region since 1949. Aside from regular chlorophyll *a* analyses and occasional taxonomic studies based on visual microscopy and HPLC pigment analysis (Hayward and Venrick, 1998; Venrick, 1992, 2002, 2009, 2012; Goericke, 2011), detailed investigations of microbial community biomass and structure have not been a part of the CalCOFI program. Beginning in November 2004, the California Current Ecosystem, Long Term Ecological Research (CCE-LTER) program has augmented core CalCOFI measurements in this area, using advanced high-throughput digital epifluorescence microscopy and flow cytometry (FCM), to assess microbial community biomass, size–structure and taxonomic composition.

Here we present for the first time a detailed examination of carbon biomass, size–structure and composition of CCE microbial communities, sampled on quarterly CalCOFI cruises from 2004 through 2010. The goal of the study is to establish baseline measurements for the southern CCE, that are relevant for documenting and investigating climate change impacts in the region, and that will facilitate the development of ecosystem models and remote sensing algorithms that capture the natural variability in phytoplankton carbon biomass and functional group composition.

2. Materials and methods

2.1. Sample collection

We collected samples for analyses of microbial community abundance, biomass and composition during 25 quarterly CalCOFI cruises from November 2004 (cruise 200411) to November 2010 (cruise 201011). On each cruise, we sampled three depths with CTD rosette casts at each of 10 'cardinal' stations distributed onshore to offshore along Lines 80 and 90 of the standard CalCOFI grid pattern (Fig. 1). The locations of cardinal stations were selected so that at least two were located in each of the major floristic regions identified by Venrick (2002, 2009). The depths of sample collection were dependent upon the depth of the in vivo fluorescence maximum: Type I stations (0–50 m fluorescence max) were sampled at 10 m as well as the middle and bottom shoulder of the fluorescence layer; Type II stations (50–80 m fluorescence max) were sampled at 10 m, 40 m and the fluorescence max; and Type III stations (80–120 m fluorescence max) were sampled at 10 m, 62 m and the fluorescence max. From each depth sampled, aliquots were taken directly from the Niskin bottles for plankton community analyses by flow cytometry (FCM) and epifluorescence microscopy, as well as for concentrations of dissolved nutrients, chlorophyll *a* (Chl *a*) and particulate organic carbon (POC) measurements made by the CalCOFI or CCE-LTER groups. Details of those methods are described below.

2.2. Analysis of eukaryotic nano- and microplankton by epifluorescence microscopy

Seawater samples (500 mL) for microscopical analysis were gently collected from the CTD and immediately preserved for slide preparation according to a modified protocol of Sherr and Sherr (1993). The samples were first preserved with 260 μL of alkaline Lugol's solution, immediately followed by 10 mL of buffered formalin and 500 μL of sodium thiosulfate, with gentle mixing between each addition. Preserved samples were shielded from light and left to rest at room temperature for 1 h. After the rest period, 1 mL of proflavin (0.33% w/v) was added and the samples were stored in the dark for an additional hour. Just prior to filtration, the preserved samples were stained with 1 mL of DAPI (0.01 mg mL^{-1}) and immediately transferred to the filtration manifold. A 50-mL aliquot (small volume, SV) of the sample was filtered through a 25-mm black polycarbonate filter with 0.8-μm pore size, and the remaining 450 mL aliquot (large volume, LV) was filtered through a 25-mm black polycarbonate filter with 8.0-μm pores. We placed a 10-μm pore size, 25-mm nylon backing filter under all polycarbonate filters to promote even cell distribution, and filtered the samples under gentle vacuum pressure (< 100 mm Hg). Each filter was then mounted onto glass slides with one drop of Type DF immersion oil and a No. 2 cover slip, and

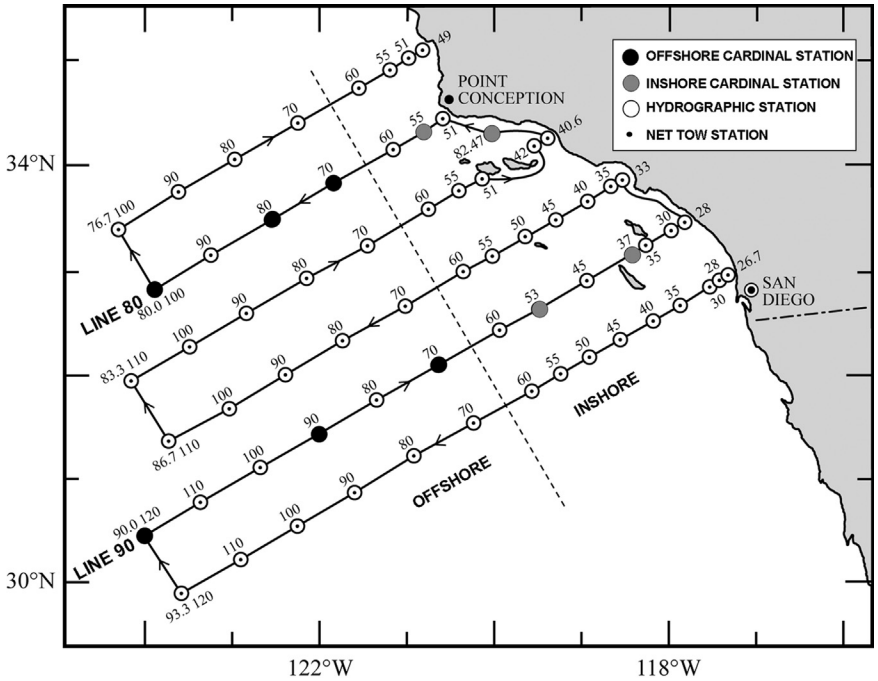

Fig. 1. Map of the CCE region showing the standard cruise tracks and station position of the CalCOFI sampling grid. The ten cardinal stations are depicted with filled in solid circles. Coastal cardinal stations are solid gray, offshore cardinal stations are solid black. Open circles are the other standard CalCOFI hydrographic stations. Map adapted from calcofi.org.

the prepared slides were frozen at −80 °C for later analysis in the lab.

Slides were digitally imaged using a Zeiss Axiovert 200 M inverted compound microscope equipped for high-throughput epifluorescence microscopy with a motorized focus drive, stage, objective and filters. Digital images were acquired with a Zeiss AxioCam MRc black and white 8-bit CCD camera. All microscope functions were controlled by Zeiss Axiovision software, and images were collected using automated image acquisition. Exposure times for each image were automatically determined by the Axiovision software to avoid over exposure. SV samples (50 mL aliquots) were viewed at 630× magnification, and LV samples (450 mL aliquots) were viewed at 200× magnification. A minimum of 20 random positions were imaged for each slide, with each position consisting of three to four fluorescent channels: Chl *a*, DAPI, FITC (SV and LV samples) and phycoerythrin (SV samples only). In addition, 5–10 *z*-plane images were acquired at each position and for each fluorescence channel. The resulting *z*-stack images were subsequently combined using an extended depth of field algorithm to produce an entirely in-focus image from each position channel for Chl *a*, DAPI and FITC. These were then false colored (Chl *a*=red, DAPI=blue and FITC=green) and combined to form a single composite 24-bit RGB image for each position (Fig. 2).

The combined images were processed and analyzed using ImagePro software to semi-automate the enumeration of eukaryotic cells larger than 1.5 µm in length (Taylor et al., 2012). Whenever possible, 20 positions and >300 cells were counted for each slide. With a VBA script routine in the ImagePro software, a series of preprocessing steps were performed using the green channel, proflavin staining of cell protein, to extract the cells from the background for measurement. The green channel was first extracted as an 8-bit gray scale image from the combined 24-bit RGB image. A fast Fourier transform was then applied to remove background noise, followed by the application of a Laplace filter to improve the definition of cell edges and to minimize the halo effects common in epifluorescent images. Poor quality images were discarded. Cells were automatically segmented from the background and outlined, and the outlines were reapplied to the original 24-bit image. User interaction was then required to check each image, split connected cells, outline cells that did not autosegment from the background and delete artifacts and detritus that the software had incorrectly outlined.

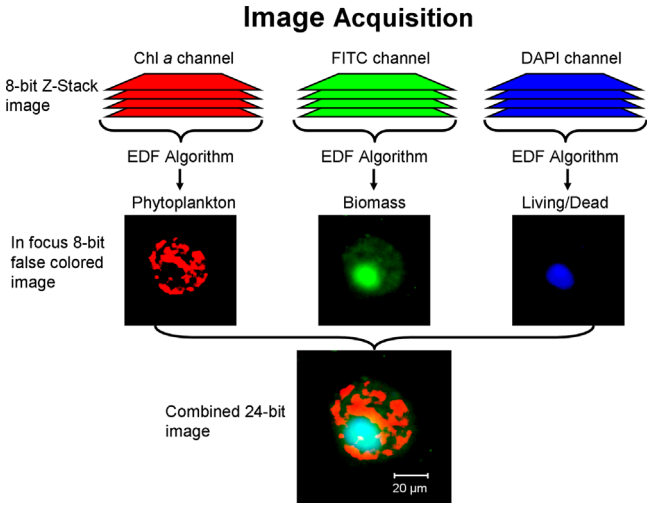

Fig. 2. A graphical illustration of the automated image acquisition process, for a single slide position using the advanced epifluorescence microscopy method. Chlorophyll *a* channel is Chl *a* autofluorescence, FITC channel is proflavin stained protein fluorescence, and DAPI channel is DAPI stained DNA fluorescence. The actual image shown for the in focus 8-bit false colored image is an autotrophic dinoflagellate under each channel, and the combined 24-bit image is three separate channels put together. (For interpretation of the references to color in this figure legend, the reader is referred to the web version of this article.)

Each cell was manually identified and grouped into seven plankton functional groups: autotrophic dinoflagellates (A-Dino), autotrophic flagellates (A-Flag), cryptophytes (Crypto), diatoms, prymnesiophytes (Prym), heterotrophic dinoflagellates (H-Dino) and heterotrophic flagellates (H-Flag). Autotrophic cells were identified by the presence of chlorophyll *a* (red autofluorescence under blue light excitation), generally clearly packaged in defined chloroplasts, and obvious heterotrophic cells with recently consumed prey were manually excluded from the autotroph classification. Although mixotrophy is a common nutritional strategy in pelagic microbial communities (Sanders, 1991; Jones, 2000; Stukel et al., 2011), mixotrophic cells are grouped with autotrophs in the present analysis. It should also be noted that because our preservation and slide-making protocols are inadequate for ciliates, they are not included in the resulting estimates of heterotrophic protist carbon (HC). As a consequence, reported HC values should be viewed as conservative estimates of protistan grazer biomass in the CCE.

Analyzed cells were grouped into three size categories (Pico, <2 µm; Nano, 2–20 µm; Micro, 20–200 µm) based on the lengths of their longest axis. The size class for autotrophic picophytoplankton (A-Pico) is dominated numerically by photosynthetic bacteria, *Prochlorococcus* (PRO) and *Synechococcus* (SYN) enumerated by FCM, but microscopy included the small eukaryotes in this size category. Biovolumes (BV; μm^3) were calculated from the length (*L*) and width (*W*) measurements of each cell using the geometric formula of a prolate sphere (BV=0.524 × LWH), assuming *H*=*W*. Biomass was calculated as carbon (*C*; pg $cell^{-1}$) using the equations of Menden-Deuer and Lessard (2000): $C=0.288\ BV^{0.811}$ for diatoms and $C=0.216\ BV^{0.939}$ for non-diatoms. These microscopical estimates of community abundance, biomass and composition are available for individual cruises at the CCE-LTER DataZoo database (http://oceaninformatics.ucsd.edu/datazoo/).

2.3. Analysis of bacterial populations by flow cytometry

Samples (2 mL) for FCM analysis of phototrophic bacteria, PRO and SYN, and heterotrophic bacteria (H-Bact) were preserved with 0.5% paraformaldehyde (final concentration) and flash frozen in liquid nitrogen. On shore, the samples were stored at −80 °C, then thawed in batches and stained with Hoechst 34442 (1 µg mL^{-1}, final concentration) immediately prior to the analysis (Campbell and Vaulot, 1993; Monger and Landry, 1993). The analyses were conducted at the SOEST Flow Cytometry Facility (www.soest.hawaii.edu/sfcf) using a Beckman-Coulter Altra flow cytometer equipped with a Harvard Apparatus syringe pump for quantitative analyses and two argon ion lasers tuned to UV (200 mW) and 488 nm (1 W) excitation. Fluorescence signals were collected using filters for Hoechst-bound DNA, phycoerythrin and chlorophyll, all normalized to internal standards of 0.5- and 1.0-µm yellow-green (YG) polystyrene beads (Polysciences Inc., Warrington, PA, USA). Listmode data files (FCS 2.0 format) of cell fluorescence and light-scatter properties were acquired with Expo32 software (Beckman-Coulter) and used with FlowJo software (Tree Star, Inc., www.flowjo.com) to define populations based on DNA signal (all cells), absence of photosynthetic pigments (H-Bact), presence of Chl *a* (PRO and SYN), presence of phycoerythrin (SYN), and forward angle light scatter (relative size). Abundance estimates from FCM analyses were converted to biomass using mixed-layer estimates of 11, 32 and 101 fg *C* $cell^{-1}$ for H-Bact, PRO and SYN, respectively (Garrison et al., 2000; Brown et al., 2008). FCM estimates of bacterial abundance

and biomass are available for individual cruises at http://oceaninformatics.ucsd.edu/datazoo/.

2.4. Chlorophyll a and POC analysis

Samples for Chl *a* and POC analyses were taken from the same hydrocasts and Niskin bottles as used for the microscopy and flow cytometry analyses.

Chlorophyll *a* values in the present dataset were obtained from the CalCOFI database (http://calcofi.org/data/ctddata.html). Analyses were done by the standard CalCOFI chlorophyll protocol (http://www.calcofi.org/references/ccmethods/292-art-chlorophyll methods.html), which is based on the methods of Yentsch and Menzel (1963), Holm-Hansen et al. (1965) and Lorenzen (1967). Briefly, seawater samples of 50–250 ml were filtered under vacuum (<500 mm Hg) onto 25-mm GF/F filters. The filters were placed in 10-ml screw top culture tubes, and the pigment was extracted in 8.0 ml of 90% acetone at -20 °C in the dark for 24–48 h. Prior to analysis, the tube contents were agitated and allowed to equilibrate to room temperature in the dark. The filters were then removed from the tubes and Chl *a* fluorescence measured on a Turner Model 10 AU fluorometer.

Particulate Organic Carbon (POC) values were obtained from the CCE-LTER DataZoo database (http://oceaninformatics.ucsd.edu/datazoo/). Seawater samples (0.5–4 L) for POC analysis were filtered onto pre-combusted 25-mm GF/F filters under low vacuum (<40 mm Hg) and stored in liquid nitrogen. In the lab, samples were acidified with fuming HCl in a desiccator, then dried for 48 h at 60 °C. Half of the filter was then placed into a 9×10-mm tin capsule and analyzed on a ESC 4010 CHNSO analyzer at 1000 °C, along with combusted GF/F blank and seven standards.

2.5. Data analyses and regional grouping

Based upon a preliminary comparison of community structure in mixed-layer samples for the ten cardinal sampling stations in Fig. 1, which agreed largely with previously established floral patterns for the southern CCE (Hayward and Venrick, 1998; Venrick, 2002, 2009), we grouped the stations into southern inshore (Stas. 90.37 and 90.53), northern inshore (Stas. 82.47 and 80.55) and offshore (Stas. 90.70, 90.90, 90.120, 80.70, 80.80, and 80.100) zones. Data from these station groupings were averaged for the 25 cruises of our study period to assess temporal variability in regional mixed-layer averages of phytoplankton community carbon biomass, size–structure, taxonomic composition and pigment concentration.

3. Results

3.1. General seasonal and spatial trends

Averaged over the six-year study period and for all mixed-layer depths sampled at each cardinal station, total biomass and composition of the phytoplankton community show the strongest seasonal differences and the highest variability between northern (Line 80) and southern (Line 90) areas at the stations closest to the coast (Figs. 3 and 4). Along Line 80 (Fig. 3), the upwelling region off Point Conception (Stn. 80.55, ~32 km offshore) had higher mean biomass during summer and fall than winter and spring cruises, while biomass in waters overlying the Santa Barbara Basin (Stn. 82.47) was higher during winter and especially springtime cruises. Along Line 90 (Fig. 4), biomass was most elevated during spring and summer cruises, with the biomass peak more typically at Stn. 90.53, rather than closer to shore (Stn. 90.37). The pattern at Stn. 90.53 likely reflects the influence of advective transport of waters from Pt. Conception upwelling to the south (Stn. 90.53, Fig. 1), as seen generally in satellite images, as well as the northward transport of subtropical waters to the innermost stations of the Southern California Bight, especially during later summer and fall (Lynn and Simpson, 1987; Venrick, 2002). Biomass at the three offshore stations along each line typically declined seaward without marked seasonal blooms, although some compositional variability was evident.

Diatoms are small contributors to biomass in the offshore stations along each line, consistent with the lack of observed seasonal blooms in these areas. Conversely, at the more inshore stations, diatoms contribute significantly to biomass, particularly during the seasons when highest total biomass for a station is observed. Diatoms, however, do not account for all of the seasonal variability observed at the more inshore stations. Notably, dinoflagellates contribute comparably or more to total biomass, on average, for most of the inshore stations and for most of the year, including the seasons of high biomass (Figs. 3 and 4). Prymnesiophytes and other flagellates also make significant contributions at times, but never clearly dominate the inshore phytoplankton assemblage at any time of the year.

As would be expected from the inshore–offshore differences in phytoplankton community composition (Figs. 3 and 4), which reflect proximity to nutrient inputs, larger cells (A-Micro, 20–200 μm) are the dominant contributors to total community biomass near the coast, and particularly near the Pt. Conception upwelling center in the north and the Santa Barbara Basin (Fig. 5). At these stations (82.55 and 80.47, respectively), A-Micro comprises 57% of total autotrophic biomass, on average, followed by A-Nano (2–20 μm cells; 38%) and A-Pico (<2-μm cells; 5%). The inshore stations on Line 90, which are substantially further offshore than their counterparts to the north, have a distinctly different size structure in which A-Nano cells typically comprise more biomass than A-Micro (Fig. 5). A-Pico cells notably maintain similar mean biomass levels (3–7 μg C L^{-1}) throughout the region, while larger cells decline significantly with distance from shore, though more so for micro- than nano-sized cells. As a consequence, A-Nano increase in relative biomass contribution, typically comprising the dominant size class (~60% of total AC), on average, at all stations except 80.55 and 82.47.

The size–structure trends for mixed-layer phytoplankton along Lines 80 and 90 are also very similar for mid and deep euphotic zone samples, although with declining carbon biomass with depth (Fig. 5). In mid-euphotic zone samples, mean biomass and size composition are almost identical to mixed-layer values at most stations, except for proportionally reduced size categories at 82.47 and 80.55. In the deep euphotic zone samples, the prominent peaks in nano- and micro-sized cells seen in the upper layers at coastal stations are greatly reduced relative to the size distributions at offshore stations.

3.2. Microbial carbon relationships to POC and chlorophyll

For all depths and stations sampled, estimates of total microbial carbon based on analyses by FCM and microscopy (MC; including all phytoplankton, heterotrophic protists and heterotrophic bacteria) account, on average, for half of the measured concentration of particulate organic carbon (POC) (Fig. 6). Very few of the microbial biomass estimates exceed measured POC, and then only by relatively small amounts. Similarly, few of the microbial biomass estimates fall significantly below 25% of POC. An ordinary least squares regression indicates that MC is related to POC by the equation $MC=0.46(POC)$, (Pearson Correlation of 0.75; $p<0.0001$).

Ratios of autotrophic carbon to chlorophyll *a* (AC:Chl *a*) for mixed-layer phytoplankton average 51.5 ± 5.3 (all errors are 95% confidence level unless otherwise noted) for the region and study

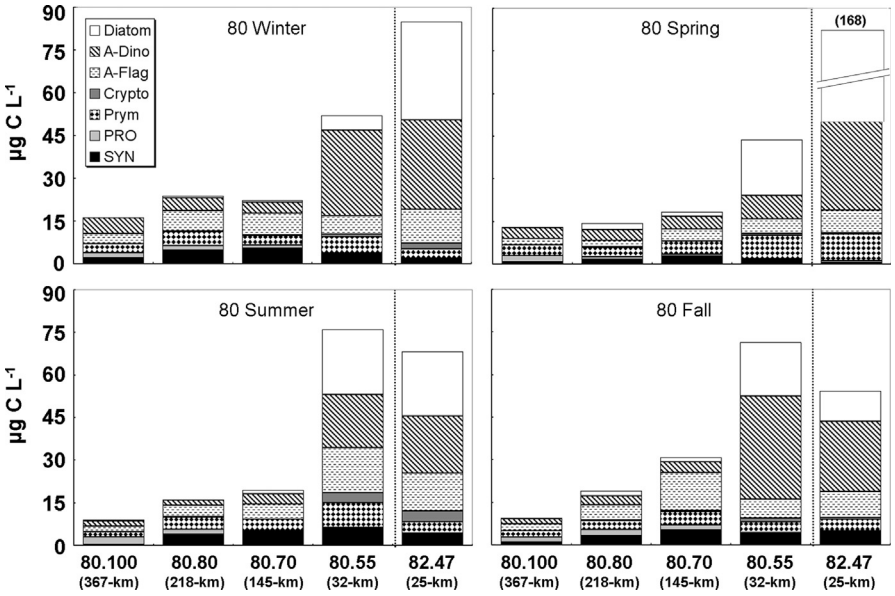

Fig. 3. Mean seasonal variations of mixed-layer phytoplankton taxa along Line 80. Diatom, autotrophic dinoflagellates (A-Dino), autotrophic flagellates (A-Flag), cryptophytes (Crypto), prymnesiophytes (Prym), *Prochlorococcus* (PRO) and *Synechococcus* (SYN). Units are µg C L^{-1}. Station numbers and distance from shore are given on the *x*-axis. Note that the bar for station 82.47 has been reduced in the spring to fit on this axis. The actual biomass concentration reached an average of 168 µg C L^{-1}, with diatoms comprising 118 µg C L^{-1} of the total community biomass. A dotted line separates the Santa Barbara Basin (station 82.47) from the rest of line 80.

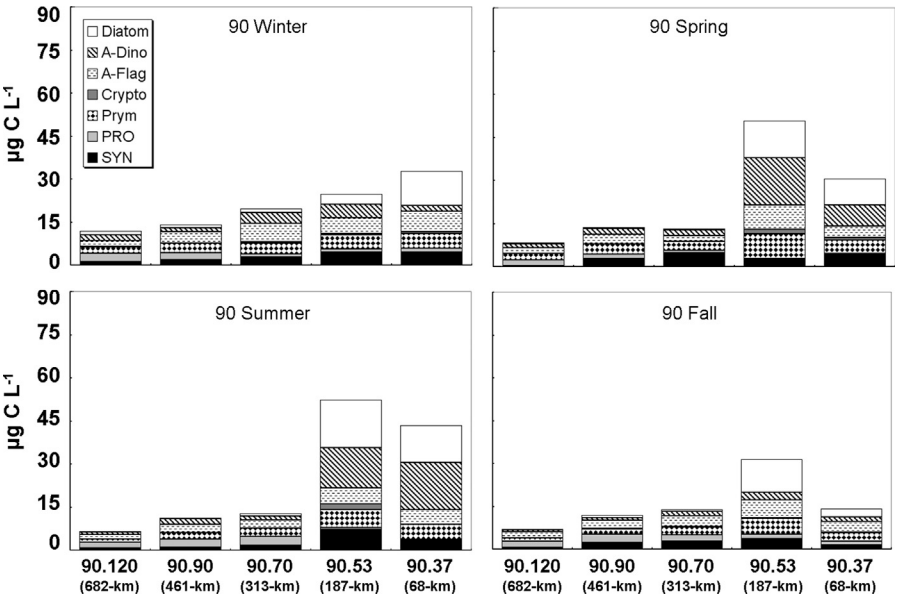

Fig. 4. Mean seasonal variations of mixed-layer phytoplankton taxa along Line 90. Diatom, autotrophic dinoflagellates (A-Dino), autotrophic flagellates (A-Flag), cryptophytes (Crypto), prymnesiophytes (Prym), *Prochlorococcus* (PRO) and *Synechococcus* (SYN). Units are µg C L^{-1}. Station numbers and distance from shore are given on the *x*-axis.

period. However, mean AC:Chl *a* in the mixed layer varies significantly with the depth of the nitracline, defined as the depth at which nitrate concentration first reaches 1 µM, for the data binned in 20-m depth intervals (Fig. 7). An ordinary least squares regression yields the relationship AC:Chl $a = 0.35 \times$ (Nitracline depth bin) + 33.48, ($R^2 = 0.90$). On average, therefore, our estimates indicate a systematic 2-fold variability in mixed-layer AC:Chl *a* ratios between the typically nearshore, upwelling influenced waters with shallow nitraclines (AC:Chl $a \approx 40$) and the typically offshore, oligotrophic waters with deep nitraclines (AC:Chl $a \approx 80$). For individual samples, however, the differences can be much greater.

Similar increasing trends of AC:Chl *a* ratio with nitracline depth are also evident for samples collected routinely in the mid and deep euphotic zone (Fig. 7), although the slopes and intercepts decline progressively with increasing depth of collection (decreasing light level, and generally higher nutrient concentrations). Like the mixed-layer, AC:Chl *a* values for the mid euphotic zone vary 2-fold, on average, from 23 to 47 for shallow and deep nitraclines, respectively. AC:Chl *a* values for the deep euphotic zone are less variable, with averages ranging from 22 to 33 from typical onshore to offshore conditions.

3.3. Temporal variability of phytoplankton biomass and composition

Over the study period, total autotrophic carbon (AC) and total chlorophyll *a* (TChl *a*) for the southern inshore CCE region each varied by about one order of magnitude, with AC ranging from 10

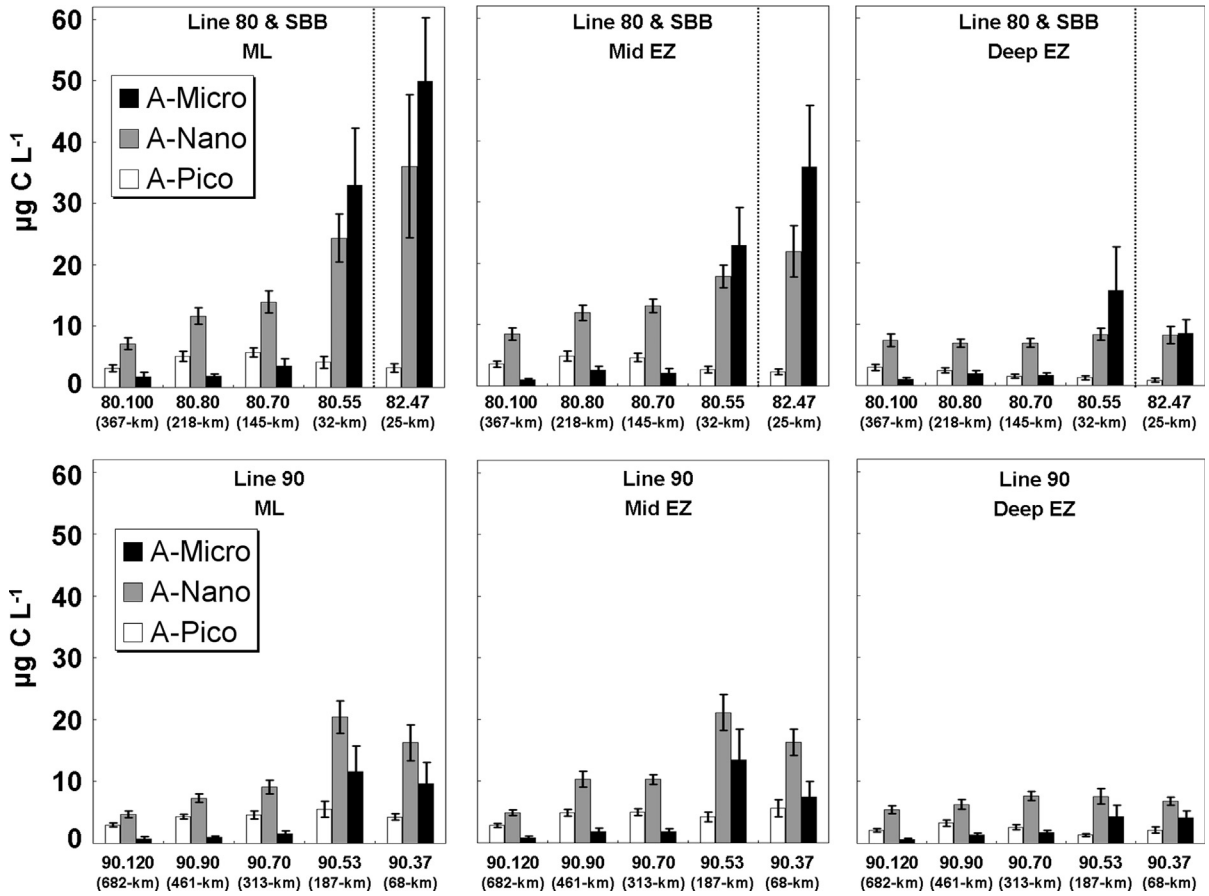

Fig. 5. Mean autotrophic community size-class structure from the mixed-layer (ML), mid euphotic zone (Mid EZ) and deep euphotic zone (Deep EZ) for the ten cardinal stations sampled during quarterly cruises from November 2004 to October 2010. Size-classes are based on the longest cell axis measured: A-Pico (0.2–2 μm), A-Nano (2–20 μm) and A-Micro (20–200 μm). Units are μg C L^{-1} and error bars represent the 95% confidence level. Station numbers and distance from shore are given on the *x*-axis. A dotted line separates the Santa Barbara Basin (station 82.47) from the rest of line 80.

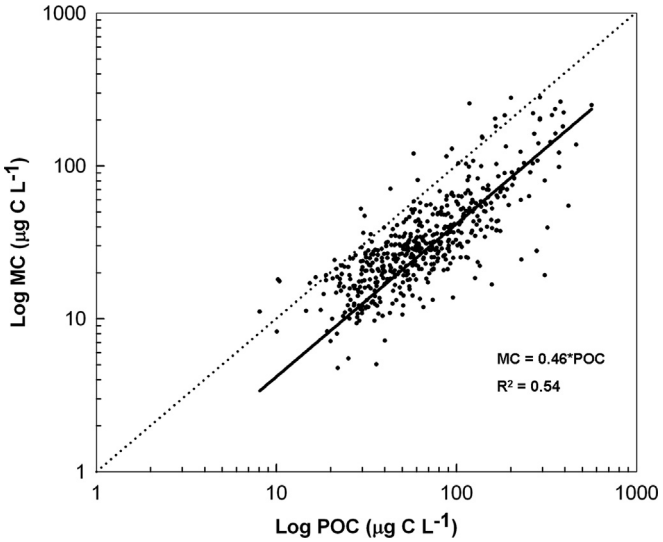

Fig. 6. Relationship between POC and total microbial carbon (MC) for all stations, depths and cruises. MC is the sum of *Prochlorococcus*, *Synechococcus*, diatom, autotrophic dinoflagellates, autotrophic flagellates, cryptophytes, prymnesiophytes, heterotrophic dinoflagellates, heterotrophic flagellates and heterotrophic bacteria. Ordinary least squares regression, $y=0.46x$, ($R^2=0.54$). The dotted line represents the 1:1 relationship.

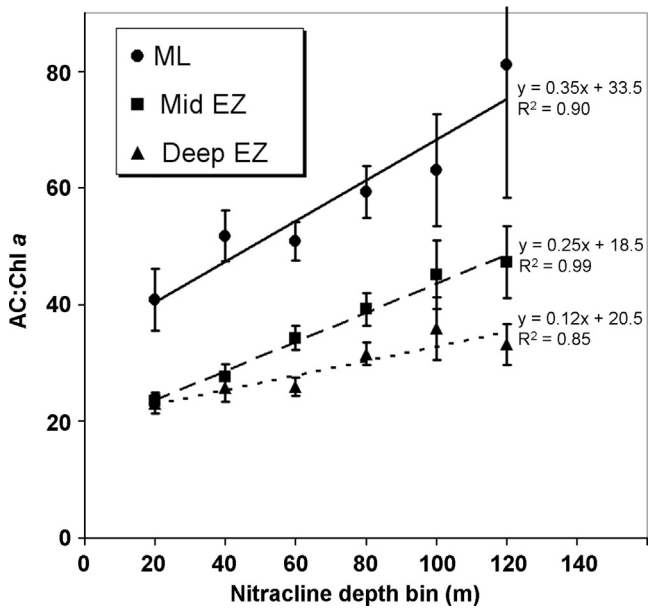

Fig. 7. Mixed layer (ML), mid euphotic zone (Mid EZ) and deep euphotic zone (Deep EZ) autotrophic carbon:chlorophyll *a* ratios (AC:Chl *a*) as a function of nitracline depth bin for all cardinal stations sampled from November 2004 to October 2010. The solid line represents an ordinary least squares (OLS) regression for the ML, the dashed line represents an OLS regression for the Mid EZ and the dotted line represents an OLS regression for the Deep EZ. Equations and R^2 values for each regression are shown next to the regression line on the plot.

to 100 μg C L^{-1} (mean 32 ± 9 μg C L^{-1}), and TChl *a* concentrations ranging from 0.18 to 3 μg Chl *a* L^{-1} (mean 0.81 ± 0.25 μg Chl *a* L^{-1}) (Table 1 and Fig. 8A). The highest concentrations of AC

Table 1
Mean biomass estimates, total chlorophyll *a* (TChl) and autotrophic carbon to chlorophyll (AC:Chl *a*) of northern inshore (stations 82.47 and 80.55), southern inshore (stations 90.37 and 90.53) and offshore (stations 80.70, 80.80, 80.100, 90.70, 90.90 and 90.120) zones from mixed-layer depths for each cruise. Diatom, autotrophic dinoflagellates (A-Dino), prymnesiophytes (Prym), cryptophytes (Crypto), autotrophic flagellates (A-Flag), *Prochlorococcus* (PRO) and *Synechococcus* (SYN). Total autotrophic carbon (AC) is the sum of all autotrophic groups. Biomass units are μg C L^{-1} and TChl units are μ gChl L^{-1}. Errors are ± the 95% confidence interval. Cruises are listed as year and month.

Region	Cruise	Biomass (μg C L^{-1})							AC	TChl	AC:Chl *a*
		Diatom	A-Dino	Prym	Crypto	A-Flag	PRO	SYN			
Northern inshore	2004-11	11 ± 2.2	120 ± 98	3.2 ± 0.3	–	4.7 ± 0.4	–	1.3 ± 0.2	100 ± 79	2.3 ± 1.0	49 ± 20
	2005-01	1.1 ± 0.5	22 ± 14	6.2 ± 1.2	–	7.8 ± 5.8	0.5 ± 0.0	1.7 ± 0.2	34 ± 18	1.8 ± 0.4	21 ± 5.5
	2005-04	82 ± 36	7.5 ± 4.8	19 ± 5.0	–	4.5 ± 1.2	1.4 ± 1.4	0.4 ± 0.1	110 ± 36	8.0 ± 4.8	18 ± 6.5
	2005-07	29 ± 5.4	2.9 ± 0.6	2.6 ± 0.3	–	7.8 ± 4.0	–	0.1 ± 0.0	42 ± 2.2	1.1 ± 0.3	42 ± 8.9
	2005-11	12 ± 7.6	160 ± 21	2.8 ± 0.1	1.4 ± 1.4	4.0 ± 0.3	–	0.5 ± 0.0	180 ± 29	0.6 ± 0.2	310 ± 70
	2006-02	11 ± 8.1	150 ± 8.1	5.2 ± 1.3	0.7 ± 0.2	7.5 ± 2.3	–	2.3 ± 0.3	170 ± 3.8	3.2 ± 0.2	55 ± 2.6
	2006-04	13 ± 12	29 ± 24	12 ± 1.3	-	6.0 ± 4.3	–	3.6 ± 2.9	63 ± 36	3.5 ± 2.6	23 ± 6.7
	2006-07	19 ± 17	71 ± 38	13 ± 5.6	10 ± 7.6	41 ± 11	–	3.7 ± 0.6	160 ± 45	3.0 ± 1.1	56 ± 6.5
	2006-10	9.1 ± 6.2	37 ± 22	2.5 ± 0.2	0.5 ± 0.5	3.4 ± 1.1	0.8 ± 0.5	3.9 ± 1.7	57 ± 32	1.4 ± 0.5	37 ± 9.0
	2007-01	28 ± 3.9	11 ± 8.5	2.7 ± 0.4	2.0 ± 1.9	5.4 ± 1.7	–	0.3 ± 0.0	49 ± 1.3	2.8 ± 0.4	18 ± 3.0
	2007-04	15 ± 10	0.7 ± 0.1	5.4 ± 1.4	1.7 ± 0.1	2.7 ± 0.2	–	0.3 ± 0.1	25 ± 9.4	1.8 ± 1.0	16 ± 4.0
	2007-07	17 ± 15	31 ± 29	4.4 ± 0.6	3.1 ± 1.2	1.7 ± 0.5	0.3 ± 0.1	3.0 ± 1.2	61 ± 46	1.2 ± 0.7	42 ± 15
	2007-11	2.9 ± 1.3	11 ± 0.8	10 ± 3.8	2.0 ± 2.0	15 ± 8.1	1.3 ± 0.2	9.2 ± 3.1	51 ± 15	2.1 ± 1.1	28 ± 7.5
	2008-01	1.4 ± 1.3	4.9 ± 1.8	6.3 ± 3.6	1.4 ± 0.6	7.8 ± 0.4	0.4 ± 0.1	3.1 ± 0.2	25 ± 5.2	1.4 ± 0.3	18 ± 0.8
	2008-04	58 ± 29	31 ± 25	3.3 ± 0.5	0.3 ± 0.3	4.9 ± 0.7	–	0.9 ± 0.1	98 ± 54	5.2 ± 2.6	18 ± 1.1
	2008-08	2.5 ± 2.5	0.9 ± 0.6	3.6 ± 0.9	0.6 ± 0.6	13 ± 1.8	0.5 ± 0.4	5.6 ± 2.3	27 ± 3.7	1.6 ± 0.4	18 ± 1.6
	2008-10	4.0 ± 3.4	0.7 ± 0.3	2.8 ± 2.5	-	16.3 ± 0.1	–	7.4 ± 2.2	31 ± 8.5	0.9 ± 0.5	43 ± 13
	2009-01	0.7	13.0	11.0	1.2	13.0	1.8	12.0	52.0	1.0	51.0
	2009-03	75 ± 68	4.6 ± 0.6	1.2 ± 0.8	3.3 ± 2.5	14 ± 3.6	–	1.2 ± 0.6	99 ± 72	5.5 ± 3.6	17 ± 2.4
	2009-07	55 ± 3.6	3.2 ± 1.5	5.8 ± 3.0	7.2 ± 7.0	7.2 ± 1.9	–	3.4 ± 0.4	81 ± 17	2.3 ± 1.2	43 ± 15
	2009-11	12 ± 8.2	4.0 ± 2.5	2.5 ± 0.2.0	1.0 ± 0.8	7.2 ± 1.4	0.2 ± 0.2	5.8 ± 1.0	33 ± 7.4	3.0 ± 2.2	20 ± 12
	2010-01	3.5 ± 2.9	2.7 ± 0.6	3.4 ± 0.1	0.8 ± 0.1	10 ± 5.2	–	1.6 ± 0.1	22 ± 8.8	1.0 ± 0.2	21 ± 3.9
	2010-04	180 ± 150	30 ± 12	4.6 ± 0.2	0.5 ± 0.5	15 ± 4.8	0.3 ± 0.3	0.3 ± 0.2	230 ± 170	11 ± 8.2	21 ± 0.1
	2010-08	15 ± 8.8	6.3 ± 1.4	8.7 ± 4.2	1.0 ± 0.9	17 ± 3.9	–	15 ± 6.3	63 ± 1.8	5.1 ± 2.7	17 ± 8.9
	2010-11	51 ± 1.7	3.4 ± 1.0	2.4 ± 0.6	1.8 ± 1.8	6.3 ± 2.1	–	2.0 ± 0.8	67 ± 1.3	3.2 ± 0.2	21 ± 0.6
Southern inshore	2004-11	0.9 ± 0.8	1.8 ± 1.0	2.6 ± 0.6	–	2.5 ± 0.4	2.6 ± 0.0	0.7 ± 0.3	11 ± 1.1	0.2 ± 0.0	63 ± 4.3
	2005-01	0.6 ± 0.1	0.3 ± 0.2	3.8 ± 0.4	–	3.4 ± 1.4	3.1 ± 0.4	3.0 ± 0.9	14 ± 1.9	0.6 ± 0.1	24 ± 2.2
	2005-04	25 ± 20	1.2 ± 0.1	2.3 ± 0.6	–	3.5 ± 0.3	0.4 ± 0.4	4.8 ± 4.2	37 ± 15	0.7 ± 0.4	59 ± 10
	2005-07	33 ± 24	56 ± 16	7.0 ± 0.7	–	1.7 ± 0.1	–	1.9 ± 1.4	99 ± 9.1	1.0 ± 0.5	120 ± 54
	2005-11	–	–	–	–	–	–	–	–	–	–
	2006-02	0.3 ± 0.1	2.8 ± 0.6	9.6 ± 1.9	0.1 ± 0.1	6.8 ± 0.3	1.4 ± 1.2	2.9 ± 1.2	24 ± 0.4	0.6 ± 0.2	53 ± 24
	2006-04	18 ± 11	41 ± 16	9.7 ± 2.5	2.9 ± 0.3	8.4 ± 6.5	-	0.9 ± 0.2	81 ± 13	3.0 ± 0.2	27 ± 6.2
	2006-07	2.5 ± 1.3	30 ± 23	12 ± 4.9	3.0 ± 2.9	9.6 ± 6.4	1.1 ± 0.4	17 ± 14	75 ± 6.1	1.2 ± 0.8	110 ± 71
	2006-10	0.1 ± 0.0	2.1 ± 0.3	1.7 ± 1.2	–	3.0 ± 1.4	2.1 ± 0.6	0.6 ± 0.1	9.5 ± 0.2	0.2 ± 0.0	45 ± 6.1
	2007-01	3.9 ± 3.1	2.7 ± 0.9	1.7 ± 0.2	0.5 ± 0.5	2.9 ± 1.8	–	1.3 ± 0.9	13 ± 7.4	0.5 ± 0.3	24 ± 2.2
	2007-04	0.8 ± 0.1	0.6 ± 0.2	8.7 ± 3.9	1.0 ± ± 1.0	5.2 ± 2.3	–	2.2 ± 0.6	19 ± 6.9	0.8 ± 0.5	32 ± 11
	2007-07	28 ± 23	2.2 ± 0.9	5.5 ± 1.4	2.8 ± 2.8	6.5 ± 0.1	0.6 ± 0.2	3.5 ± 0.8	49 ± 27	1.9 ± 1.5	37 ± 14
	2007-11	0.9 ± 0.7	6.6 ± 3.7	5.0 ± 2.7	1.1 ± 0.7	5.7 ± 3.9	–	3.2 ± 1.6	23 ± 13	1.1 ± 0.5	18 ± 4.3
	2008-01	1.2 ± 0.6	5.0 ± 1.0	8.3 ± 4.2	1.1 ± 1.1	13 ± 7.3	0.4 ± 0.1	6.5 ± 1.2	35 ± 11	1.2 ± 0.6	32 ± 6.7
	2008-04	10 ± 6.7	1.6 ± 1.1	4.0 ± 2.0	1.1 ± 0.1	6.0 ± 1.7	–	1.5 ± 1.1	24 ± 0.6	1.5 ± 0.0	16 ± 0.1
	2008-08	0.3 ± 0.1	–	1.7 ± 0.2	–	5.4 ± 1.9	0.8 ± 0.8	1.6 ± 0.1	9.9 ± 1.5	0.3 ± 0.0	37 ± 0.9
	2008-10	34 ± 30	–	1.9 ± 0.3	–	6.4 ± 0.2	–	2.7 ± 1.7	45 ± 31	0.7 ± 0.5	67 ± 1.6
	2009-01	3.3 ± 0.3	11 ± 7.4	7.0 ± 2.2	0.2 ± 0.2	9.4 ± 2.3	0.4 ± 0.4	7.3 ± 1.5	39 ± 10	0.8 ± 0.1	50 ± 4.2
	2009-03	0.5 ± 0.1	2.1 ± 1.0	2.4 ± 0.9	–	6.0 ± 0.5	2.3 ± 1.2	6.7 ± 1.8	20 ± 1.7	0.5 ± 0.1	44 ± 4.2
	2009-07	24 ± 9.9	2.4 ± 0.6	3.1 ± 0.7	–	3.0 ± 1.2	0.2 ± 0.2	2.1 ± 1.1	35 ± 9.5	0.4 ± 0.1	96 ± 4.3
	2009-11	–	0.8 ± 0.7	3.0 ± 2.1	–	3.3 ± 1.5	1.0 ± 0.2	4.6 ± 1.8	13 ± 6.4	0.3 ± 0.1	35 ± 8.3
	2010-01	0.1 ± 0.0	0.8 ± 0.0	2.9 ± 0.6	0.4 ± 0.4	3.8 ± 1.0	0.8 ± 0.2	6.1 ± 4.8	15 ± 6.5	0.4 ± 0.1	35 ± 11
	2010-04	1.5 ± 1.3	4.1 ± 1.8	6.3 ± 1.8	0.5 ± 0.5	7.9 ± 0.3	1.5 ± 0.4	4.4 ± 1.9	26 ± 4.6	0.5 ± 0.1	54 ± 0.8
	2010-08	1.0 ± 0.9	1.1 ± 0.7	5.2 ± 2.0	–	6.0 ± 1.5	0.3 ± 0.3	5.5 ± 2.4	19 ± 6.0	0.5 ± 0.0	36 ± 8.4
	2010-11	8.0 ± 4.6	1.6 ± 0.3	11 ± 3.9	–	9.0 ± 0.4	2.5 ± 0.6	3.4 ± 1.9	36 ± 0.9	0.7 ± 0.1	50 ± 8.0
Offshore	2004-11	2.7 ± 2.2	1.4 ± 0.3	2.0 ± 0.5	–	9.8 ± 5.7	2.9 ± 0.7	1.7 ± 0.7	20 ± 6.1	0.5 ± 0.2	72 ± 18
	2005-01	0.6 ± 0.3	4.6 ± 1.3	2.2 ± 0.5	–	3.8 ± 0.6	3.0 ± 0.5	4.9 ± 1.8	19 ± 3.3	0.5 ± 0.2	48 ± 7.7

Table 1 (*continued*)

Region	Cruise	Biomass (μg C L^{-1})							AC	TChl	AC:Chl *a*
		Diatom	A-Dino	Prym	Crypto	A-Flag	PRO	SYN			
	2005-04	1.4 ± 0.7	3.4 ± 1.1	3.1 ± 0.7	–	1.5 ± 0.2	1.2 ± 0.4	0.8 ± 0.3	11 ± 2.7	0.2 ± 0.0	130 ± 47
	2005-07	0.1 ± 0.0	2.1 ± 0.6	4.2 ± 0.7	–	1.4 ± 0.6	2.4 ± 0.6	1.0 ± 0.6	11 ± 1.8	0.4 ± 0.1	30 ± 5.8
	2005-11	0.1 ± 0.1	2.0 ± 0.7	3.8 ± 1.0	0.1 ± 0.1	2.3 ± 0.6	2.1 ± 0.3	2.7 ± 1.8	13 ± 3.8	0.4 ± 0.1	33 ± 4.1
	2006-02	-	1.6 ± 0.3	3.5 ± 0.6	–	1.9 ± 0.5	1.7 ± 0.5	1.0 ± 0.4	9.7 ± 1.3	0.3 ± 0.1	40 ± 7.4
	2006-04	0.3 ± 0.1	2.9 ± 1.2	4.0 ± 0.8	–	1.7 ± 0.5	1.9 ± 0.6	1.8 ± 0.8	13 ± 2.0	0.2 ± 0.0	85 ± 18
	2006-07	0.3 ± 0.1	1.4 ± 0.4	1.9 ± 0.7	–	1.8 ± 0.5	3.4 ± 0.9	2.4 ± 1.5	11 ± 2.5	0.3 ± 0.1	56 ± 12
	2006-10	0.2 ± 0.1	0.9 ± 0.2	1.4 ± 0.4	–	2.2 ± 0.3	3.0 ± 0.4	0.4 ± 0.1	8.0 ± 1.0	0.2 ± 0.0	60 ± 13
	2007-01	15 ± 14	3.4 ± 1.1	2.7 ± 0.9	0.8 ± 0.4	4.6 ± 1.5	2.9 ± 0.6	2.0 ± 0.9	32 ± 13	0.8 ± 0.2	40 ± 6.8
	2007-04	1.4 ± 0.8	1.4 ± 0.5	4.1 ± 0.6	0.2 ± 0.2	2.6 ± 0.7	1.4 ± 0.9	1.1 ± 0.4	12 ± 2.2	0.4 ± 0.1	50 ± 13
	2007-07	1.3 ± 0.5	1.2 ± 0.4	3.7 ± 0.8	–	2.4 ± 0.4	2.7 ± 0.6	0.3 ± 0.1	12 ± 1.5	0.2 ± 0.1	100 ± 18
	2007-11	1.4 ± 0.7	4.2 ± 1.6	2.8 ± 0.7	0.3 ± 0.3	3.2 ± 0.9	1.9 ± 0.5	3.7 ± 1.5	18 ± 4.4	0.4 ± 0.1	48 ± 9.4
	2008-01	0.7 ± 0.3	3.2 ± 1.5	5.0 ± 0.7	0.3 ± 0.1	4.6 ± 0.9	1.3 ± 0.7	3.0 ± 1.1	18 ± 3.8	0.6 ± 0.1	32 ± 4.6
	2008-04	7.6 ± 4.1	3.7 ± 0.9	3.8 ± 0.6	0.3 ± 0.1	5.0 ± 0.8	0.9 ± 0.5	1.8 ± 0.5	23 ± 4.2	0.8 ± 0.3	44 ± 9.0
	2008-08	0.5 ± 0.2	0.8 ± 0.5	1.2 ± 0.2	0.1 ± 0.0	4.6 ± 1.1	0.2 ± 0.2	1.9 ± 0.4	9.4 ± 1.5	0.2 ± 0.0	44 ± 6.0
	2008-10	3.2 ± 1.6	0.8 ± 0.4	1.8 ± 0.4	–	6.6 ± 2.1	-	1.5 ± 0.5	14 ± 4.6	0.3 ± 0.1	47 ± 4.5
	2009-01	0.6 ± 0.3	8.6 ± 3.2	5.7 ± 0.7	0.3 ± 0.2	5.9 ± 1.0	1.8 ± 0.2	4.1 ± 1.3	27 ± 5.5	0.5 ± 0.1	53 ± 3.9
	2009-03	1.1 ± 0.4	1.2 ± 0.5	2.2 ± 0.4	–	6.5 ± 1.8	1.1 ± 0.2	1.5 ± 0.3	14 ± 2.8	0.3 ± 0.1	40 ± 3.4
	2009-07	0.3 ± 0.1	4.4 ± 1.2	2.7 ± 0.7	0.1 ± 0.1	3.8 ± 0.5	0.9 ± 0.2	2.1 ± 0.7	14 ± 2.8	0.2 ± 0.0	79 ± 4.9
	2009-11	0.3 ± 0.2	1.0 ± 0.3	3.2 ± 1.5	0.5 ± 0.2	4.5 ± 1.2	1.4 ± 0.3	2.9 ± 1.0	14 ± 3.9	0.5 ± 0.2	36 ± 4.9
	2010-01	-	1.5 ± 0.6	2.4 ± 1.0	–	9.1 ± 2.8	1.7 ± 0.1	3.7 ± 1.2	18.5 ± 5	0.4 ± 0.1	44 ± 3.3
	2010-04	3.8 ± 3.3	6.0 ± 2.4	2.8 ± 0.4	0.2 ± 0.2	5.6 ± 1.2	0.8 ± 0.3	5.3 ± 2.1	24 ± 6.5	0.7 ± 0.4	59 ± 8.7
	2010-08	0.7 ± 0.6	1.6 ± 1.2	2.4 ± 0.5	0.3 ± 0.3	4.5 ± 1.6	3.1 ± 0.8	4.2 ± 2.4	17 ± 4.9	0.3 ± 0.1	64 ± 6.6
	2010-11	0.7 ± 0.6	5.2 ± 2.1	4.7 ± 1.3	0.5 ± 0.3	7.4 ± 3.2	3.3 ± 0.6	5.0 ± 2.2	27 ± 8.6	0.5 ± 0.2	64 ± 6.6

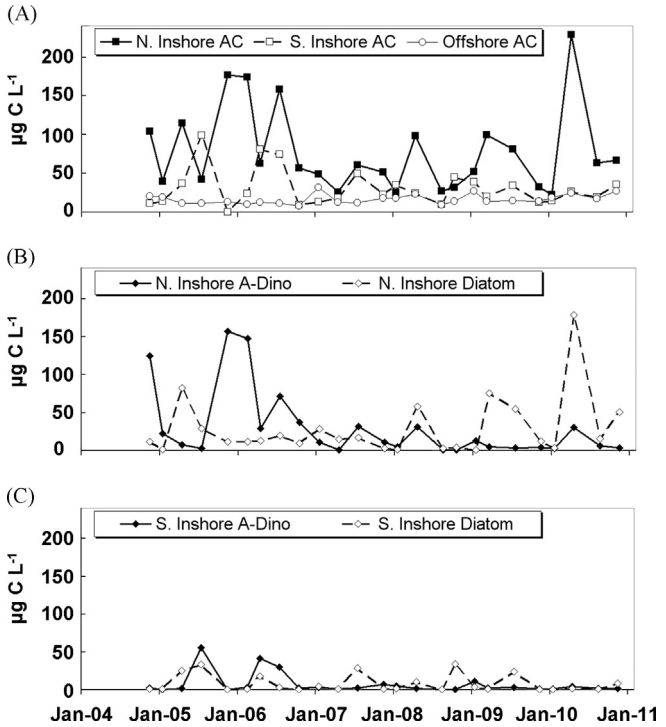

Fig. 8. (A) Mixed-layer biomass of total autotrophic carbon (AC) from November 2004 to October 2010. Offshore stations, northern inshore stations (N.) and southern inshore stations (S.). (B) Mixed-layer biomass of northern inshore autotrophic dinoflagellates (A-Dino) and diatoms. (C) Mixed-layer biomass of southern inshore A-Dino and diatoms. Units are μg C L^{-1}.

were measured in July 2005 and the highest TChl *a* were measured in April 2006, while the lowest values were found in October 2006 (AC) and November 2004 (TChl *a*). For the northern inshore CCE region AC and TChl *a* also varied by about one order of magnitude, with AC ranging from 22 to 229 μg C L^{-1} (mean 78 ± 22 μg C L^{-1}), and TChl *a* ranging from 0.64 to 11 μg Chl *a* L^{-1} (mean 3.0 ± 0.95 μg Chl *a* L^{-1}) (Table 1 and Fig. 8A). The highest concentrations of AC and TChl *a* were measured in April 2010, while the lowest values of AC were found in January 2010, and November 2005 (TChl *a*). Biomass concentrations were distinctly lower and less variable in the offshore zone, ranging from 8.0 to 32.0 μg C L^{-1} (mean 16.4 ± 2.4 μg C L^{-1}) for AC (Fig. 8A) and from 0.15 to 0.80 μg Chl *a* L^{-1} (mean 0.40 ± 0.07 μg Chl *a* L^{-1}) for TChl *a* (Table 1).

Community composition by taxonomic groups differed substantially between the inshore and offshore environments. For the northern inshore stations, phytoplankton biomass was dominated by autotrophic dinoflagellates (A-Dino) and diatoms (Table 1 and Fig. 8B), which comprised an average of 39% and 36% of AC, respectively. Temporally, dinoflagellates were the most dominant group earlier in the study period, particularly during 2005 and 2006, while diatoms predominated later (Fig. 8B). Other contributors to autotrophic carbon biomass varied temporally in the northern inshore zone, but decreased on average in order from autotrophic flagellates (A-Flag; 13%), prymnesiophytes (Prym; 7%), *Synechococcus* (SYN; 5%), cryptophytes (Crypto; 2%) to *Prochlorococcus* (PRO; < 1%).

Among the southern inshore stations, phytoplankton biomass was dominated by diatoms and A-Dino (Table 1 and Fig. 8C), which comprised 26% and 23% of AC, respectively, on average. A-Dino were also the most dominant group earlier in the study period for the southern inshore zone, particularly during 2005 and 2006, while diatoms predominated later (Fig. 8C). Other contributors to AC biomass varied temporally in the southern inshore zone, but

decreased on average from A-Flag (18%) to Prym (16%), SYN (12%), PRO (3%) and Crypto (2%). Phytoplankton community biomass in the offshore region of the CCE was more evenly distributed among the functional groups, with AF comprising 26%, Prym 19%, A-Dino 17%, SYN 15%, PRO 12%, diatoms 11% and Crypto 1% of mixed-layer AC biomass (Table 1).

3.4. Temporal variability of heterotrophic protists

The distributions of heterotrophic protists (HC) assessed by epifluorescence microscopy, comprised of heterotrophic dinoflagellates (H-Dino) and heterotrophic flagellates (H-Flag), generally follow the biomass patterns for AC, except from late 2005 to early 2006 (Fig. 9A). As noted previously, since biomass of mixotrophs and ciliates are not included in our estimates of heterotrophic protist carbon, the reported values are conservative. For the northern inshore stations, HC varied by a factor of 18, with a mean concentration of 17.8 ± 6.1 μg C L^{-1} (Fig. 9B). The highest concentrations (61.2 μg C L^{-1}) were found during October 2006, while the lowest concentrations (3.3 μg C L^{-1}) were during July 2007. The ratio of total AC to HC for these stations ranged from 1 to 29, with a mean value of 6.8 ± 2.6.

For the southern inshore zone of the CCE, HC varied by a factor of 9, averaging 9.2 ± 1.9 μg C L^{-1} (Fig. 9C). The highest HC concentration (24.1 μg C L^{-1}) was in April 2006, while the lowest (2.6 μg C L^{-1}) was in April 2007. The ratio of total AC to HC for the southern inshore stations averaged 3.6 ± 0.8 and was less variable than the northern inshore zone, ranging from 1 to 10.

For the offshore regions of the CCE, HC was slightly more stable, varying by a factor of 5.8, and had a mean concentration of 6.8 ± 1.2 μg C L^{-1} (Fig. 9A). The highest HC value (15.3 μg C L^{-1}) was found during January 2009, while the lowest (2.6 μg C L^{-1}) was in October 2006. The ratio of AC to HC in the offshore CCE ranged from 1 to 6, with a mean value of 2.6 ± 0.4.

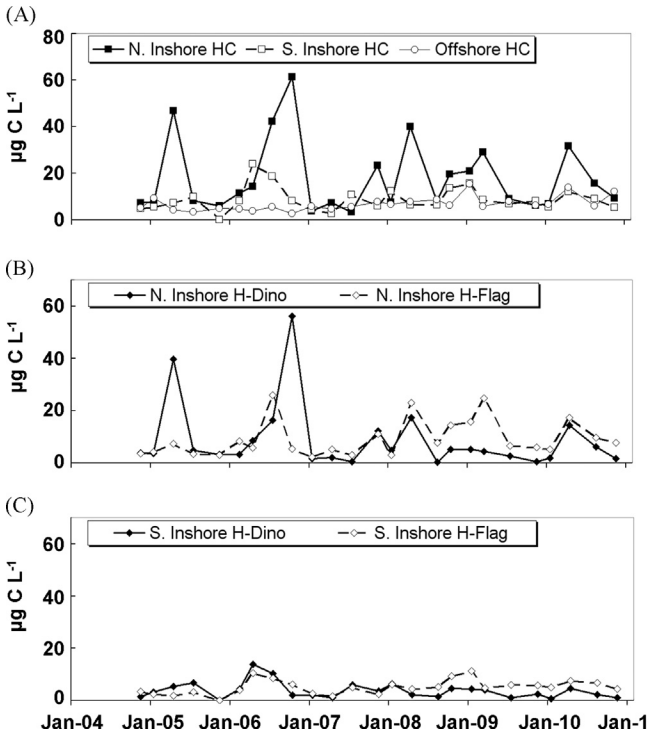

Fig. 9. (A) Mixed-layer biomass of total heterotrophic protist carbon (HC) from November 2004 to October 2010. Offshore stations, northern inshore stations (N.) and southern inshore stations (S.). (B) Mixed-layer biomass of northern inshore heterotrophic dinoflagellates (H-Dino) and heterotrophic flagellates (H-Flag). (C) Mixed-layer biomass of southern inshore H-Dino and H-Flag. Units are μg C L^{-1}.

4. Discussion

4.1. Seasonal phytoplankton trends

Coastal upwelling and wind stress curl are major drivers of the nutrient inputs that support phytoplankton production and biomass in the southern CCE (Legaard and Thomas, 2006; Rykaczewski and Checkley, 2008; Mantyla et al., 2008; Thomas et al., 2009). Nutrient mixing by winter storms, followed by periods of relative calm and sunshine, can also fuel significant wintertime production in the latitudinal range (30–35°N) of the CalCOFI grid. These seasonal and areal differences in nutrient delivery mechanisms, along with relatively consistent year-round ocean conditions, lead to a poorly defined seasonal bloom cycle for the southern CCE as a whole. In addition, a recent weakening of spring blooms in the region, as noted by the shift to more summer phytoplankton maxima after the major El Niño event in 1997–98 (Venrick, 2012), might contribute to reduced seasonality in the present data.

A spring biomass maximum is only evident for station 82.47 overlying the Santa Barbara Basin, which also has relatively high biomass in the winter (Table 1 and Fig. 3). Large April blooms of diatoms in this area have long been known (Allen, 1945a, 1945b). However, at Stn. 80.55, 32 km off Pt. Conception, which is more strongly influenced by the seasonal cycle of coastal upwelling favorable winds, biomass is highest during the summer and fall. Spring–summer differences are less well defined in the south, although mean phytoplankton biomasses for both of the shoreward stations on Line 90 increase during the summer (Table 1 and Fig. 4). This area is enriched by wind-stress curl, by advective transport from Pt. Conception upwelling, and by eddies, fronts and meanders of the California Current jet, which takes an eastward turn toward the coast in this vicinity (Lynn and Simpson, 1987; Hayward et al., 1995; Peláez and McGowan, 1986; Thomas and Strub, 1990; Haury et al., 1993; Venrick, 2000; Taylor et al., 2012).

Generally, mean phytoplankton biomass in the offshore stations is highest during wintertime, although the enhancement is no greater than a factor of two compared to other seasons (Figs. 3 and 4). In subtropical North Pacific waters to the west, a winter maximum in surface chlorophyll concentration has long been noted (Letelier et al., 1993; Venrick, 1993; Winn et al., 1995), though largely ascribed to a photoadaptive response of cellular pigment to lower seasonal light (Letelier et al., 1993). Additionally, Yuras et al. (2005) have reported a winter increase in chlorophyll concentration in the offshore surface waters in the southern Pacific off the coast of Chile. Our current study, as well as a recent similar analysis of phytoplankton samples collected by the Hawaii Ocean Time-series Program at Station ALOHA (Pasulka et al., 2013), document that the winter chlorophyll maximum is more than a pigment response, but an actual seasonal, though modest, increase in carbon biomass of the plankton community.

4.2. Microbial carbon relationships to POC

Particulate organic carbon (POC) measurements provide an upper-limit constraint on estimates of total microbial carbon (MC; including all phytoplankton, heterotrophic protists and heterotrophic bacteria) from our microscopy and FCM analyses. For all stations, depths and cruises, our samples of MC average one half of POC, and only a few of the MC samples were less than 25% of POC. One conclusion that we can draw from this result is that the carbon:biovolume conversion factors used in our analyses do not produce large and obvious systematic errors in plankton biomass estimates. It is also apparent that relationships among living organisms (MC), non-living particles (detritus) and total POC are surprisingly consistent across quite variable environmental conditions in the CCE.

Cho and Azam (1990) observed a similar constancy between POC estimates and phytoplankton and bacterial carbon in environments ranging from the oligotrophic North Pacific gyre to the coastal Southern California Bight. However, their study did not include heterotrophic protists, and it used a carbon to chlorophyll *a* conversion of 47–50 to estimate phytoplankton carbon. Using similar microscopy-based assessments of protistan biomass to those used here, Landry et al. (2002) also noted that plankton carbon estimates in the Southern Ocean were consistently around a mean of 58% of POC for varying conditions, from open ocean to ice-edge blooms. In addition, Claustre et al. (1999) estimated that detrital material contributed between 43% and 55% of total euphotic-layer particles in the tropical Pacific, using particle attenuation as a proxy for POC, relative to chlorophyll in situ fluorescence. Such results suggest that there exist, at least on regional scales, a general balance of living and non-living particulate carbon across a broad range of system states.

4.3. Autotrophic carbon to chlorophyll ratios

The mean autotrophic carbon to chlorophyll *a* (AC:Chl *a*) value of 51.5 ± 5.3 determined in this study is only slightly lower than the widely used value of 58 derived by Eppley et al. (1992) from the slope of the regression of POC versus total chlorophyll *a* (TChl *a*) for samples taken in the equatorial Pacific. While is it reassuring to see that these estimates are not much different, the value of the present data is not in validating a mean number, but in guiding appropriate usage of variable AC:Chl *a* values in experimental, modeling and remote sensing studies of the CCE. Many factors affect AC:Chl *a* values, including light, nutrients, temperature, taxonomic composition, growth rate and time of day (Eppley et al., 1971; Eppley, 1972; Cullen, 1982; Geider, 1987). In addition, methodological imprecisions, notably from inadequate counts of large rare cells with high individual carbon contents, introduce substantial errors into the ratio calculations. Since such errors balance out in large data sets, our results are best viewed as providing broad mean estimates of how the ratio varies spatially within the southern CCE region, rather than precise individual estimates of ratio variability.

Mean trends in the CCE data show strong associations between AC:Chl *a* and nitracline depth for all depth strata sampled (Fig. 7). The taxonomic and size-class composition of the different communities of the CCE also play a role in these AC:Chl *a* trends. For example, diatoms have lower AC:Chl *a* values than autotrophic dinoflagellates, and larger cells typically have lower AC:Chl *a* than smaller cells (Chan, 1980; Falkowski et al., 1985; Geider, 1987). Therefore, coastal communities dominated by large diatoms are expected to have lower AC:Chl *a* values. Although the mean values of AC:Chl *a* largely reflect variability along environmental gradients from the eutrophic nearshore (shallow nitracline) to oligotrophic offshore (deep nitracline), they also predict how values might respond, for example, to depression of the nitracline during El Niño events, or to temporal variability at a given location due to local processes or advective transport of water by jets, eddies, current meanders or other mechanisms. In general, variations in nitracline depth within the CCE lead to a factor of two difference in mixed-layer AC:Chl *a* values. There is another 2-fold difference, on average, between near-surface and deep euphotic zone values at a given location (Fig. 7).

Although AC:Chl *a* is rarely measured, both its values and its variability are important for estimating carbon flows from pigment-based experimental rate determinations (e.g., Landry et al., 2009; Stukel et al. 2013), for modeling of ocean ecosystem dynamics (Morel, 1988; Taylor et al., 1991; Sathyendranath et al., 2009; Wang et al., 2009) and for interpreting biomass and production distributions with remote sensing techniques (Eppley et al., 1985; Falkowski, 1994; Antoine et al., 1996; Behrenfled et al., 2005). Using CCE-LTER data, for example, Li et al. (2010) have successfully parameterized models that effectively capture observed spatial and depth variability in phytoplankton biomass, AC:Chl *a* and growth rates across inshore and offshore regions of the southern CCE. In more general usage, values in the range of 20–80, appropriate for the conditions measured (Fig. 7), will better account for the natural variability of AC:Chl *a* encountered in the southern CCE region.

4.4. Community composition

Microbial communities of the CCE vary by location and season from low biomass, mixed communities of small pico- and nano-sized cells to high biomass assemblages dominated by large microplankton, often a single taxon or functional group. The former, characteristic of the offshore region, has greater taxonomic evenness than the inshore sampling stations and greater relative contribution (28%) of phototrophic bacteria (Figs. 3 and 4). In terms of size–structure and composition, the offshore CCE assemblages resemble those in oligotrophic regions of the central Pacific, although with higher biomass concentrations and substantially reduced dominance of cells in the pico-phytoplankton size class. Nonetheless, taxonomic analysis of larger cells by Venrick (1992, 2002, 2009) has shown that species composition in offshore CCE waters is very similar to that of the North Pacific subtropical gyre (NPSG). Additionally, using the same methods as the current study, Pasulka et al. (2013) found similar phytoplankton community composition at station ALOHA in the NPSG, which would reasonably constitute the oligotrophic end-member of CCE variability.

For the inshore regions of the CCE, high nutrient delivery by coastal upwelling (Huyer, 1983; Jones et al., 1983), results in blooms of diatoms or A-Dinos, which overprint the ubiquitous background assemblage of smaller taxa (Figs. 3, 4 and 8B). Diatoms dominate the northern inshore phytoplankton community during most years and seasons. However, autotrophic dinoflagellates were especially prevalent in our data from late 2004 and mid 2005 to mid 2006 (Fig. 8B). While conditions in the CalCOFI–CCE study area during this time period were not extraordinary, and near their long-term averages, the upwelling season in the northern California Current was markedly delayed, creating unusually warm sea surface temperatures through the spring and early summer months (Hickey et al., 2006; Peterson et al., 2006; Schwing et al., 2006; Barth et al., 2007). High dinoflagellate biomass during this period was not just a local phenomenon for the inshore region of the southern CCE. Dominant toxin-producing algal species in central California shifted from diatoms to dinoflagellates (Jester et al., 2009), and there were also reports of reduced zooplankton biomass, reduced seabird fecundity and altered marine mammal foraging in more northern waters (Peterson et al., 2006; Sydeman et al., 2006; Weise et al., 2006). Additionally, northern anchovy densities decreased significantly from 2005 to 2006 off the Oregon and Washington coast, and fatty acid biomarkers of northern anchovy, Pacific herring and whitebait smelt indicated that the food web in 2005 was mainly based on dinoflagellates, switching back to diatoms in 2006 (Litz, 2008; Litz et al., 2008).

Our present study of the microbial community biomass, size–structure and composition is the first of its kind for the CCE region. While the resulting six-year dataset is too short to detect long-term trends, it nevertheless establishes baseline measurements that will help to document and resolve temporal trends in future CCE and CalCOFI sampling. The present study also provides a robust dataset to facilitate the development and testing of ecosystem models at the level of phytoplankton functional groups and to improve algorithms for extracting community biomass and composition information from satellite remote sensing measurements. Future climate changes

in the southern CCE region are projected to include increased thermal stratification (Rykaczewski and Dunne, 2010), increased delivery of nitrate to coastal areas by upwelling (Bakun, 1990; Snyder et al., 2003; Aksnes and Ohman, 2009), and increased number and intensity of ocean frontal systems (Kahru et al., 2012), each capable individually of significantly impacting productivity, standing stocks and composition of the food web base, though their effects will likely differ spatially. Continued monitoring as well as experimental and modeling studies are needed to elucidate how such changes will combine to alter biogeochemical cycling and trophic coupling within the southern CCE region.

Acknowledgments

We would like to thank the CCE-LTER technicians Megan Roadman and Shonna Dovel for collecting samples during the quarterly CalCOFI/CCE-LTER cruises, and the CalCOFI team for providing chlorophyll, POC and hydrographic data. Additionally, we gratefully acknowledge James Conners and the CCE-LTER DataZoo team for their help in putting together the large dataset used for this study. This work was funded by U. S. National Science Foundation grants OCE 04-17616 and 10-26607 for the CCE-LTER Program.

References

Aksnes, D.L., Ohman, M.D., 2009. Multi-decadal shoaling of the euphotic zone in the southern sector of the California Current System. Limnol. Oceanogr. 54, 1272–1281.

Allen, W.E., 1945a. Seasonal Occurrence of Marine Plankton Diatoms of Southern California in 1938. Contributions of Scripps Institution of Oceanography. New Series. No. 45, pp. 293–334.

Allen, W.E., 1945b. Vernal Distribution of Marine Plankton Diatoms Offshore in Southern California in 1940. Contributions of Scripps Institution of Oceanography. New Series. No. 2585, pp. 335–369.

Antoine, D., André, J.-M., Morel, A., 1996. Oceanic primary production 2. Estimation at global scale from satellite (coastal zone color scanner) chlorophyll. Glob. Biogeochem. Cycles 10, 57–69.

Bakun, A., 1990. Global climate change and intensification of coastal ocean upwelling. Science 247, 198–201.

Barth, J.A., Menge, B.A., Lubchenco, J., Chan, F., Bane, J.M., Kirincich, A.R., McManus, M.A., Nielsen, K.J., Pierce, S.D., Washburn, L., 2007. Delayed upwelling alters nearshore coastal ocean ecosystems in the Northern California Current. Proc. Natl. Acad. Sci. 104, 3719–3724.

Behrenfled, M.J., Boss, E., Siegel, D.A., Shea, D.M., 2005. Carbon-based ocean productivity and phytoplankton physiology from space. Glob. Biogeochem. Cycles 19, GB1006, http://dx.doi.org/10.1029/2004GB002299.

Bray, N.A., Keyes, A., Morawitz, W.M.L., 1999. The California Current system in the Southern California Bight and the Anta Barbara Channel. J. Geophys. Res. 104, 7695–7714.

Brown, S.L., Landry, M.R., Yang, E.J., Rii, Y.M., Bidigare, R.R., 2008. Diatoms in the desert: plankton community response to a mesoscale eddy in the subtropical North Pacific. Deep-Sea Res. II 55, 1321–1333.

Campbell, L., Vaulot, D., 1993. Photosynthetic picoplankton community structure in the subtropical North Pacific Ocean near Hawaii (station ALOHA). Deep-Sea Res. I 40, 2043–2060.

Chan, A.T., 1980. Comparative physiological study of marine diatoms and dinoflagellates in relation to irradiance and cell size. II. Relationship between photosynthesis, growth, and carbon/chlorophyll *a* ratio. J. Phycol. 16, 428–432.

Cho, B.C., Azam, F., 1990. Biogeochemical significance of bacterial biomass in the ocean's euphotic zone. Mar. Ecol. Prog. Ser. 63, 253–259.

Claustre, H., Morel, A., Babin, M., Cailliau, C., Marie, D., Martym, J.-C., Tailliez, D., Vaulot, D., 1999. Variability in particle attenuation and chlorophyll fluorescence in the tropical Pacific: scales, patterns, and biogeochemical implications. J. Geophys. Res. 104, 3401–3422.

Cullen, J.J., 1982. The deep chlorophyll maximum: comparing vertical profiles of chlorophyll *a*. Can. J. Fish. Aquat. Sci. 39, 791–803.

Di Lorenzo, E., Miller, A.J., Neilson, D.J., Cornuelle, B.D., Moisan, J.R., 2004. Modelling observed California Current mesoscale eddies and the ecosystem response. Int. J. Remote Sens. 25, 1307–1312.

Eppley, R.W., Carlucci, A.F., Holm-Hansen, O., Kiefer, D., McCarthy, J.J., Venrick, E., Williams, P.M., 1971. Phytoplankton growth and composition in shipboard cultures supplied with nitrate, ammonium, or urea as the nitrogen source. Limnol. Oceanogr. 16, 741–751.

Eppley, R.W., 1972. Temperature and phytoplankton growth in the sea. Fish. Bull. (U.S.) 70, 1063–1085.

Eppley, R.W., Stewart, E., Abbott, M.R., Heyman, U., 1985. Estimating ocean primary production from satellite chlorophyll. Introduction to regional differences and statistics for the Southern California Bight. J. Plankton Res. 7, 57–70.

Eppley, R.W., Chavez, F.P., Barber, R.T., 1992. Standing stocks of particulate carbon and nitrogen in the equatorial Pacific at 150°W. J. Geophys. Res. 97, 655–661.

Falkowski, P.G., Dubinsky, Z., Wayman, K., 1985. Growth-irradiance relationships in phytoplankton. Limnol. Oceanogr. 30, 311–321.

Falkowski, P.G., 1994. The role of phytoplankton photosynthesis in global biogeochemical cycles. Photosynth. Res. 39, 235–258.

Garrison, D.L., Gowing, M.M., Hughes, M.P., Campbell, L., Caron, D.A., Dennett, M.R., Shalapyonok, A., Olson, R.J., Landry, M.R., Brown, S.L., Liu, H., Azam, F., Steward, G.F., Ducklow, H.W., Smith, D.C., 2000. Microbial food web structure in the Arabian Sea: a US JGOFS study. Deep-Sea Res. II 47, 1387–1422.

Geider, R.J., 1987. Light and temperature dependence of the carbon to chlorophyll *a* ratio in microalgae and cyanobacteria: implications for physiology and growth of phytoplankton. New Phytol. 106, 1–34.

Goericke, R., 2011. The structure of marine phytoplankton communities – patterns, rules and mechanisms. CalCOFI Rep. 52, 182–197.

Gruber, N., Frenzel, H., Doney, S.C., Marchesiello, P., McWilliams, J.C., Moisan, J.R., Oram, J.J., Plattner, G.-K., Stolzenbach, K.D., 2006. Eddy-resolving simulation of plankton ecosystem dynamics in the California Current System. Deep-Sea Res. I 53, 1483–1516.

Haury, L.R., Venrick, E.L., Fey, C.L., McGowan, J.A., Niiler, P.P., 1993. The Ensenada front: July 1985. CalCOFI Rep. 34, 69–88.

Hayward, T.L., Venrick, E.L., 1998. Nearsurface pattern in the California Current: coupling between physical and biological structure. Deep-Sea Res. II 45, 1617–1638.

Hayward, T.L., Cayan, D.R., Franks, P.J.S., Lynn, R.J., Mantyla, A.W., McGowan, J.A., Smith, P.E., Schwing, F.B., Venrick, E.L., 1995. The state of the California Current in 1994–1995: a period of transition. CalCOFI Rep. 36, 19–39.

Hickey, B., 1979. The California Current system – hypotheses and facts. Prog. Oceanogr. 8, 191–279.

Hickey, B., MacFadyen, A., Cochlan, W., Kudela, R., Bruland, K., Trick, C., 2006. Evolution of chemical, biological, and physical water properties in the Northern California Current in 2005: remote or local wind forcing? Geophys. Res. Lett. 33, L22S02, http://dx.doi.org/10.1029/2006GL026782.

Holm-Hansen, O., Lorenzen, C.J., Holms, R.W., Strickland, J.D.H., 1965. Fluorometric determination of chlorophyll. J. Conseil Int. Explor. Mer. 30, 3–15.

Huyer, A., 1983. Coastal upwelling in the California Current System. Prog. Oceanogr. 12, 259–284.

Jester, R., Lefebvre, K., Langlois, G., Vigilant, V., Baugh, K., Silver, M.W., 2009. A shift in the dominant toxin-producing algal species in central California alters phycotoxins in food webs. Harmful Algae 8, 291–298.

Jones, B.H., Brink, K.H., Dugdale, R.C., Stuart, D.W., Ven Leer, J.C., Blasco, D., Kelley, J.C., 1983. Observations of a persistent upwelling center off Point Conception, California. In: Suess, E., Thiede, J. (Eds.), Coastal Upwelling, Its Sediment Record. Part A: Responses of the Sedimentary Regime to Present Coastal Upwelling. Plenum Press, New York, pp. 37–60

Jones, R.I., 2000. Mixotrophy in planktonic protists: an overview. Freshw. Biol. 45, 219–226.

Kahru, M., Di Lorenzo, E., Manzano-Sarabia, M., Mitchell, G.B., 2012. Spatial and temporal statistics of sea surface temperature and chlorophyll fronts in the California Current. J. Plankton Res. 34, 749–760.

Kahru, M., Lee, Z., Kudela, R.M., Manzano-Sarabia, M., Mitchell, G.B., 2015. Multi-satellite time series of inherent optical properties in the California Current. Deep-Sea Research II 112, 19–106, http://dx.doi.org/10.1016/j.dsr2.2013.07.023.

Landry, M.R., Ohman, M.D., Goericke, R., Stukel, M.R., Tsyrklevich, K., 2009. Lagrangian studies of phytoplankton growth and grazing relationships in a coastal upwelling ecosystem off Southern California. Prog. Oceanogr. 83, 208–216.

Landry, M.R., Selph, K.E., Brown, S.L., Abbott, M.R., Measures, C.I., Vink, S., Allen, C.B., Calbet, A., Christensen, S., Nolla, H., 2002. Seasonal dynamics of phytoplankton in the Antarctic Polar Front region at 170°W. Deep-Sea Res. II 49, 1843–1865.

Legaard, K.R., Thomas, A.C., 2006. Spatial patterns in seasonal and interannual variability of chlorophyll and sea surface temperature in the California Current. J. Geophys. Res. 111, C06032, http://dx.doi.org/10.1029/2005JC003282.

Letelier, R.M., Bidigare, R.R., Hebel, V., Ondrusek, M., Winn, C.D., Karl, D.M., 1993. Temporal variability of phytoplankton community structure based on pigment analysis. Limnol. Oceanogr. 38, 1420–1437.

Li, Q.P., Franks, P.J.S., Landry, M.R., Goericke, R., Taylor, A.G., 2010. Modeling phytoplankton growth rates and chlorophyll to carbon ratios in the California coastal and pelagic ecosystems. J. Geophys. Res. 115, 1–12.

Litz, M.N.C., 2008. Ecology of the Northern Subpopulation of Northern Anchovy (*Engraulis mordax*) in the California Current Large Marine Ecosystem (Master's thesis). Retrieved from ⟨http://hdl.handle.net/1957/8313⟩.

Litz, N.M.C., Heppell, S.S., Emmett, R.L., Brodeur, R.D., 2008. Ecology and distribution of the northern subpopulation of northern anchovy (*Engraulis mordax*) off the U.S. west coast. CalCOFI Rep. 49, 167–182.

Lorenzen, C.J., 1967. Determination of chlorophylls and phaeopigments: spectrophotometric equations. Limnol. Oceanogr. 12, 343–346.

Lynn, R.J., Simpson, J.J., 1987. The California Current system: the seasonal variability of its physical characteristics. J. Geophys. Res. 92, 12947–12966.

Mantyla, A.W., Bograd, S.J., Venrick, E.L., 2008. Patterns and controls of chlorophyll *a* and primary productivity cycles in the Southern California Bight. J. Mar. Syst. 73, 48–60.

Menden-Deuer, S., Lessard, E.J., 2000. Carbon to volume relationships for dinoflagellates, diatoms and other protist plankton. Limnol. Oceanogr. 45, 569–579.

Monger, B.C., Landry, M.R., 1993. Flow cytometric analysis of marine bacteria with Hoechst 33342. Appl. Environ. Microbiol. 59, 905–911.
Morel, A., 1988. Optical modeling of the upper ocean in relation to its biogenous matter content (Case I Waters). J. Geophys. Res. 93, 10749–10768.
Niiler, P.P., Poulain, P.-M., Haury, L.R., 1989. Synoptic three-dimensional circulation in an onshore-flowing filament of the California Current. Deep-Sea Res. 36, 385–405.
Pasulka, A.L., Landry, M.R., Taniguchi, D.A.A., Taylor, A.G., Church, M.J., 2013. Temporal dynamics of phytoplankton and heterotrophic protists at station ALOHA. Deep-Sea Res. II
Peláez, J., McGowan, J.A., 1986. Phytoplankton pigment patterns in the California Current as determined by satellite. Limnol. Oceanogr. 31, 927–950.
Peterson, B., Emmett, R., Goericke, R., Venrick, E., Mantyla, A., Bograd, S.J., Schwing, F.B., Ralston, S., Forney, K.A., Hewitt, R., Lo, N., Watson, W., Barlow, J., Lowry, M., Lavaniegos, B.E., Chavez, F., Sydeman, W.J., Hyrenbach, D., Bradley, R.W., Warzybok, P., Hunter, K., Benson, S., Weise, M., Harvey, J., 2006. The state of the California current, 2005–2006: warm in the north, cool in the south. Calif. Coop. Ocean. Fish. Invest. Rep. 47, 30–74.
Rykaczewski, R.R., Checkley, D.M., 2008. Influence of ocean winds on the pelagic ecosystem in upwelling regions. Proc. Natl. Acad. Sci. 105, 1965–1970.
Rykaczewski, R.R., Dunne, J.P., 2010. Enhanced nutrient supply to the California Current Ecosystem with global warming and increased stratification in an earth system model. Geophys. Res. Lett. 37, L21606, http://dx.doi.org/10.1029/2010GL045019.
Sanders, R.W., 1991. Mixotrophic protists in marine and fresh-water ecosystems. J. Protozool. 38, 76–81.
Sathyendranath, S., Stuart, V., Nair, A., Oka, K., Nakane, T., Bouman, H., Forget, M.-H., Maass, H., Platt, T., 2009. Carbon-to-chlorophyll ratio and growth rate of phytoplankton in the sea. Mar. Ecol. Prog. Ser. 383, 73–84.
Schwing, F.B., Bond, N.A., Bograd, S.J., Mitchell, T., Alexander, M.A., Mantua, N., 2006. Delayed coastal upwelling along the U.S. West Coast in 2005: a historical perspective. Geophys. Res. Lett. 33, L22S01, http://dx.doi.org/10.1029/2006GL026911.
Sherr, E.B., Sherr, B.F., 1993. Preservation and storage of samples for enumeration of heterotrophic protists. In: Kemp, P.K. (Ed.), Handbook of Methods in Aquatic Microbial Ecology. CRC Press, Boca Raton, FL, pp. 207–212
Snyder, M.A., Sloan, L.C., Diffenbaugh, N.S., Bell, J.L., 2003. Future climate change and upwelling in the California Current. Geophys. Res. Lett. 30, http://dx.doi.org/10.1029/2003GL017647.
Stukel, M.R., Landry, M.R., Selph, K.E., 2011. Nanoplankton mixotrophy in the eastern equatorial Pacific. Deep-Sea Res. II 58, 378–386.
Stukel, M.R., Décima, M., Selph, K.E., Taniguchi, D.A.A., Landry, M.R., 2013. The role of *Synechococcus* in vertical flux in the Costa Rica upwelling dome. Prog. Oceanogr.
Sydeman, W.J., Bradley, R.W., Warzybok, P., Abraham, C.L., Jahncke, J., Hyrenbach, K.D., Kousky, V., Hipfner, J.M., Ohman, M.D., 2006. Planktivorous auklet *Ptychoramphus aleuticus* responds to ocean climate 2005, unusual atmospheric blocking? Geophys. Res. Lett. 33, LS22S09, http://dx.doi.org/10.1029/2006GL026736.
Taylor, A.G., Goericke, R., Landry, M.R., Selph, K.E., Wick, D.A., Roadman, M.J., 2012. Sharp gradients in phytoplankton community structure across a frontal zone in the California Current Ecosystem. J. Plankton Res. 34, 778–798.
Taylor, A.H., Watson, A.J., Ainsworth, M., Robertson, J.E., Turner, D.R., 1991. A modeling investigation of the role of phytoplankton in the balance of carbon at the surface of the north Atlantic. Glob. Biogeochem. Cycles 5, 151–171.
Thomas, A.C., Strub, P.T., 1990. Seasonal and interannual variability of pigment concentrations across a California Current frontal zone. J. Geophys. Res. 95, 13023–13042.
Thomas, A.C., Brickley, P., Weatherbee, R., 2009. Interannual variability in chlorophyll concentrations in the Humboldt and California Current systems. Prog. Oceanogr. 83, 386–392.
Venrick, E.L., 1992. Phytoplankton species structure in the central North Pacific: is the edge like the center? J. Plankton Res. 14, 665–680.
Venrick, E.L., 1993. Phytoplankton seasonality in the central North Pacific: the endless summer reconsidered. Limnol. Oceanogr. 38, 1135–1149.
Venrick, E.L., 2000. Summer in the Ensenada Front: the distribution of phytoplankton species, July 1995 and September 1988. J. Plankton Res. 22, 813–841.
Venrick, E.L., 2002. Floral patterns in the California Current System off Southern California: 1990–1996. J. Mar. Res. 60, 171–189.
Venrick, E.L., 2009. Floral patterns in the California Current: the coastal-offshore boundary zone. J. Mar. Res. 67, 89–111.
Venrick, E.L., 2012. Phytoplankton in the California Current system off southern California: changes in a changing environment. Prog. Oceanogr. 104, 46–58.
Wang, X., Le Borgne, R., Murtugudde, R., Busalacchi, A.J., Behrenfeld, M., 2009. Spatial and temporal variability of the phytoplankton carbon to chlorophyll ratio in the equatorial Pacific: a basin-scale modeling study. J. Geophys. Res. 114, C07008, http://dx.doi.org/10.1029/2008JC004942.
Weise, M.J., Costa, D.P., Kudela, R.M., 2006. Movement and diving behavior of male California sea lion (*Zalophus californianus*) during anomalous oceanographic conditions of 2005 compared to those of 2004. Geophys. Res. Lett. 33, LS22S10, http://dx.doi.org/10.1029/2006GL027113.
Winn, C.D., Campbell, L., Christian, J.R., Letelier, R.M., Hebel, D.V., Dore, J.E., Fujieki, L., Karl, D.M., 1995. Seasonal variability in the phytoplankton community of the North Pacific Subtropical Gyre. Glob. Biogeochem. Cycles 9, 605–620.
Yentsch, C.S., Menzel, D.W., 1963. A method for the determination of phytoplankton chlorophyll and phaeophytin by fluorescence. Deep-Sea Res. 10, 221–231.
Yuras, G., Ulloa, O., Hornazábal, S., 2005. On the annual cycle of coastal and open ocean satellite chlorophyll off Chile (18°–40°S). Geophys. Res. Lett. 32, L23604, http://dx.doi.org/10.1029/2005GL023946.